

Anomalous transport resolved in space and time by fluorescence correlation spectroscopy

Felix Höfling^{ab*}, Karl-Ulrich Bamberg^b, and Thomas Franosch^{bc}

Received: May 22, 2018

A ubiquitous observation in crowded cell membranes is that molecular transport does not follow Fickian diffusion but exhibits subdiffusion. The microscopic origin of such a behaviour is not understood and highly debated. Here we discuss the spatio-temporal dynamics for two models of subdiffusion: fractional Brownian motion and hindered motion due to immobile obstacles. We show that the different microscopic mechanisms can be distinguished using fluorescence correlation spectroscopy (FCS) by systematic variation of the confocal detection area. We provide a theoretical framework for space-resolved FCS by generalising FCS theory beyond the common assumption of spatially Gaussian transport. We derive a master formula for the FCS autocorrelation function, from which it is evident that the beam waist of an FCS experiment is a similarly important parameter as the wavenumber of scattering experiments. These results lead to scaling properties of the FCS correlation for both models, which are tested by *in silico* experiments. Further, our scaling prediction is compatible with the FCS half-value times reported by Wawrezinieck *et al.* [Biophys. J. 89, 4029 (2005)] for *in vivo* experiments on a transmembrane protein.

Key words: single-molecule techniques, diffusion of macromolecules, random processes, molecular crowding

Introduction

Measurement of molecular transport at the subcellular level can provide important information on both physiological mechanisms and physical interactions that drive and constrain biochemical processes. The obstructed motion of biomolecules in living cells displays anomalous transport including subdiffusion, which was established in the past decade by numerous experiments applying techniques with labeled particles. Nevertheless, the interpretation of the collected data remains often controversial and the origin of the subdiffusive behaviour is highly debated.^{1–6} Crowded environments like cellular membranes contain structures on many length scales, and further progress depends on experimental techniques that resolve transport on these different scales. Such spatio-temporal information is needed to test and refine models of anomalous transport.

One widespread technique for the investigation of molecular transport is fluorescence correlation spectroscopy (FCS), which follows the motion of fluorescently labeled molecules with high temporal resolution.^{7,8} This mesoscopic, local method consists of collecting the fluorescent light from a steadily illuminated volume or area and autocorrelating its intensity fluctuations. An important parameter of FCS measurements is the beam waist of the illumination laser. While experimental setups in the past were constrained to a fixed value, recent technological advancements allow large variations of the confocal detection area to gather spatial informa-

tion.^{9–14} By z-scan FCS^{9,10} or beam expanders,¹¹ focal radii can be varied between 200 nm and 500 nm, but measurements at the nanoscale became possible by introducing nano-apertures (75 nm to 250 nm).¹² Only lately, a far-field optical nanoscopic method named stimulated emission depletion (STED) fluorescence correlation microscopy was developed to beat the diffraction limit,¹³ allowing focal radii to span almost a decade down to 15 nm (Ref. 14).

The subdiffusive motion of macromolecules in crowded cells and membranes was studied extensively by FCS experiments^{15–18} and was complemented in real-space by single-particle tracking.^{19–22} For Fickian diffusion, the mean-square displacement grows linearly in time, $\delta r^2(t) = 4Dt$ in two dimensions with diffusion constant D . Then, the decay of the FCS autocorrelation function obeys

$$G(t) = \frac{1}{N} \frac{1}{1 + t/\tau_D}, \quad (1)$$

where $\tau_D = w^2/4D$ denotes the dwell time and N the average number of labeled molecules in the illuminated area.[†] These equations are no longer valid for anomalous transport. Introducing the walk dimension d_w , subdiffusion is characterised by $\delta r^2(t) \sim t^{2/d_w}$, and FCS experiments are often rationalised by

$$G(t) = \frac{1}{N} \frac{1}{1 + (\Gamma t)^\alpha} \quad (2)$$

upon fitting N , Γ , and α . It is usually and tacitly anticipated that both exponents coincide, $\alpha = 2/d_w$.

Here, we provide a theoretical framework for space-resolved FCS. Relating the FCS function $G(t)$ to the intermediate scattering

^aRudolf Peierls Centre for Theoretical Physics, 1 Keble Road, Oxford OX1 3NP, England, United Kingdom

^bArnold Sommerfeld Center for Theoretical Physics (ASC) and Center for Nano Science (CeNS), Fakultät für Physik, Ludwig-Maximilians-Universität München, Theresienstraße 37, 80333 München, Germany

^cInstitut für Theoretische Physik, Friedrich-Alexander-Universität Erlangen-Nürnberg, Staudtstraße 7, 91058 Erlangen, Germany

*Present address: Max-Planck-Institut für Metallforschung, Heisenbergstraße 3, 70569 Stuttgart and Institut für Theoretische und Angewandte Physik, Universität Stuttgart, Pfaffenwaldring 57, 70569 Stuttgart, Germany

[†]We restrict the discussion to two dimensional systems relevant for membranes, where focus distortions are negligible; in three dimensions, the asphericity of the illumination volume renders the formulae more cumbersome. We also ignore effects due to the photophysics of the dye molecules, which are relevant at very short time scales only. This does not effect the generality of our discussion nor any of our conclusions.

function, we generalise the conventionally used fit models and connect FCS to time-resolved scattering techniques. If the beam waist is considered an adjustable experimental parameter similar to the scattering angle, FCS is turned into a valuable tool for the investigation of complex and in particular anomalous transport. The new approach greatly facilitates *in silico* experiments: for two models of subdiffusion, we show how spatio-temporal information on the tracer dynamics can be obtained and used to distinguish different mechanisms as the origin of anomalous transport.

Theory

Generalised FCS theory. Let us briefly revisit the theory underlying the FCS technique;^{8,23} we specialise to two dimensions for simplicity. The detection area is illuminated by a laser beam with intensity profile $W(\mathbf{r})$. The fluorescent light depends on the fluctuating, local concentration $c(\mathbf{r}, t)$ of labeled molecules in the laser focus. Thus, the intensity collected at the detector is a spatially weighted average, $I(t) \propto \int d^2r W(\mathbf{r}) c(\mathbf{r}, t)$. The output of the FCS experiment is the time-autocorrelation function of the intensity fluctuation $\delta I(t) = I(t) - \langle I \rangle$ around the mean intensity. It is conventionally normalised as $G(t) = \langle \delta I(t) \delta I(0) \rangle / \langle I \rangle^2$; proper normalisation would be achieved by multiplication with $N = \langle I \rangle^2 / \langle \delta I^2 \rangle$. Introducing spatial Fourier transforms, one arrives at the representation

$$G(t; w) = \frac{1}{N} \frac{\int d^2q |W(\mathbf{q})|^2 S(\mathbf{q}, t)}{\int d^2q |W(\mathbf{q})|^2 S(\mathbf{q}, t=0)}, \quad (3)$$

where $S(\mathbf{q}, t) = \int d^2r \exp(i\mathbf{q} \cdot \mathbf{r}) \langle \delta c(\mathbf{r}, t) \delta c(\mathbf{0}, 0) \rangle$ is known as the intermediate scattering function and $W(\mathbf{q})$ denotes the Fourier transform of the intensity profile $W(\mathbf{r})$.

An conventional laser emits a Gaussian beam profile, $W(\mathbf{r}) \propto \exp(-2r^2/w^2)$, with beam waist w , which implies a Gaussian filter function $|W(\mathbf{q})|^2 \propto \exp(-q^2 w^2/4)$. Usually only a small fraction of the molecules is labeled, and then $S(\mathbf{q}, t)$ reduces to the incoherent intermediate scattering function

$$S(\mathbf{q}, t) \approx F(\mathbf{q}, t) = \langle \exp(i\mathbf{q} \cdot \Delta \mathbf{R}(t)) \rangle. \quad (4)$$

Considering the displacements $\Delta \mathbf{R}(t) := \mathbf{R}(t) - \mathbf{R}(0)$ after a fixed time lag a random variable, the incoherent scattering function can be interpreted as their characteristic function. For Gaussian and isotropic displacements, $\langle \Delta \mathbf{R}(t) \rangle = 0$, only the second cumulant $\delta r^2(t) := \langle |\Delta \mathbf{R}(t)|^2 \rangle$ is non-zero. Thus $F(\mathbf{q}, t) = \exp(-q^2 \delta r^2(t)/4)$ for two-dimensional motion. The corresponding FCS function is calculated to

$$G_{\text{Gauss}}(t; w) = \frac{1}{N} \frac{1}{1 + \delta r^2(t)/w^2}. \quad (5)$$

For normal diffusion, it holds $F(\mathbf{q}, t) = \exp(-Dq^2 t)$, and $G(t)$ attains the simple form of Eq. (1). For the case of subdiffusion, $\delta r^2(t) \sim t^\alpha$, and Gaussian spatial displacements as in fractional Brownian motion (FBM), one recovers the conventional expression, Eq. (2).

In many complex systems, however, the (strong) assumption of Gaussian displacements is not valid and may only serve as an approximation. This assumption can be tested experimentally by resolving the spatial properties of the particle trajectories. An exact

expression for the FCS function is obtained by combining equations (3) and (4). Evaluating the integrals over the wavenumber yields

$$G(t; w) = N^{-1} \left\langle \exp(-\Delta \mathbf{R}(t)^2/w^2) \right\rangle, \quad (6)$$

which is a central result of our work. Let us emphasise that it does not require any assumptions on the dynamics; corrections may arise from non-dilute labeling of the molecules and from deviations of the Gaussian beam profile. In three-dimensional systems, one should further correct for anisotropies in the confocal volume. This expression enables new insight in the potential of the FCS technique with consequences for the design of future FCS experiments. The similarity of the representation of $G(t; w)$ in Eq. (6) with that of $F(k, t)$ in Eq. (4) suggests that FCS encodes important spatial information analogous to scattering methods like photon correlation spectroscopy or neutron spin echo. In the case of anomalous transport discussed below, we will use it as starting point for the derivation of the scaling properties of $G(t; w)$. Equation (6) shows that the FCS function $NG(t)$ can be neatly interpreted as the return probability for a fluorescent molecule to be again (or still) in the illuminated area.[‡] As a by-product, it provides a simple description for the efficient evaluation of autocorrelated FCS data in computer simulations, circumventing the evaluation of the rapidly fluctuating fluorescent light intensity.

Van Hove correlation function. The dynamics of a single labeled particle is encoded in the probability distribution of the time-dependent displacements, $P(\mathbf{r}, t) = \langle \delta(\mathbf{r} - \mathbf{R}(t)) \rangle$; due to rotational symmetry, it actually depends merely on the magnitude $r = |\mathbf{r}|$. This function is also known as van Hove (self-)correlation function $G(r, t)$ in the field of liquid dynamics;²⁴ to avoid confusion with the FCS function, we follow the notation of Ref. 25. Explicit expressions for $P(r, t)$ exist for many models, but for the dynamics on percolation clusters only conjectures of the asymptotic scaling behaviour are available. Let us consider a random walker on the incipient infinite percolation cluster, i.e., precisely at the percolation threshold. Then, the dynamics is characterised by two universal exponents: the fractal dimension d_f and the walk dimension d_w . Let further t_0 and σ denote the typical microscopic time and length scales, respectively. The van Hove function is expected to obey the following scaling law for $r \gg \sigma$ and $t \gg t_0$ (Ref. 25),

$$P_\infty(r, t) = r^{-d} \widehat{P}_\infty(r t^{-1/d_w}). \quad (7)$$

The subscript ∞ indicates that the average is taken only for tracers on the infinite cluster. During a time t , the walker explores regions of linear extension of the order of $R \sim t^{1/d_w}$. The probability for larger excursions decreases rapidly (presumably like a stretched exponential), hence we assume $\widehat{P}_\infty(x \gg 1) \rightarrow 0$ rapidly. This property specifies the time evolution of the mean-square displacement and of higher moments. For the FCS measurements, however, we additionally need the limiting behaviour of the scaling function for small arguments.

[‡]For sufficiently large time lag, the probability to find the fluorophore at a particular point within the confocal volume becomes independent of the position. Then, the FCS function can be approximated by the probability of being at or returning to the centre of the confocal volume after the given time multiplied by the size of the confocal volume.

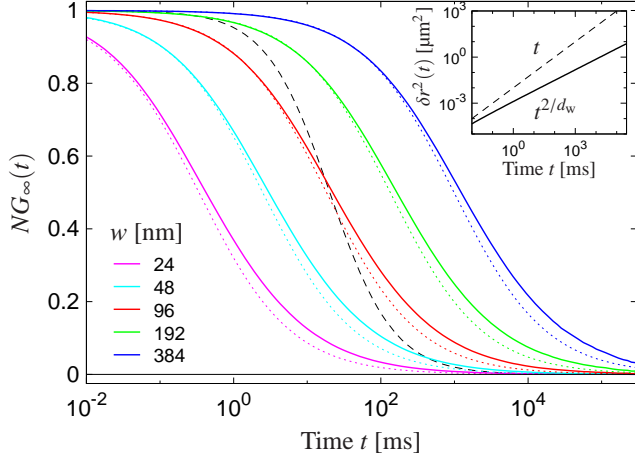


Fig. 1: Simulated FCS correlation function $G_\infty(t)$ on a logarithmic time axis for tracers on the infinite cluster at the critical obstacle density; the beam waist w of the laser increases from left to right. Dotted lines correspond to FBM with identical mean-square displacement, Eq. (5); the broken line displays the FCS function for unobstructed, normal diffusion ($w = 450$ nm). Inset: subdiffusive behaviour of the mean-square displacement for the simulated obstructed motion (solid line), again compared to the case of normal diffusion (broken line).

Return probability. Integrating the van Hove function over distances $r \leq w$ with w much larger than any microscopic length yields the probability $\Pi(t; w)$ to return to the starting point of the random walk within a radius w after a time t . Provided that $w \ll t^{1/d_w}$, this probability is proportional to the accessible part of the illuminated area, which scales as w^{d_t} . In particular, we expect that space- and time-dependence factorise,

$$\Pi(t; w) = \int_{r \leq w} d^d r P_\infty(r, t) \sim w^{d_t} \Pi_0(t), \quad (8)$$

where $\Pi_0(t)$ denotes the return probability to an infinitesimal vicinity of the origin. By the scaling law Eq. (7), we require that $\widehat{P}_\infty(x \ll 1) \sim x^{d_t}$, which is confirmed by our simulations for the two-dimensional Lorentz model. As a by-product, one obtains $\Pi_0(t) \sim t^{-d_t/d_w} = t^{-d_s/2}$, where $d_s = 2d_t/d_w$ is the *spectral dimension*. Combining both results, $\Pi(t; w) \sim (wt^{-1/d_w})^{d_t}$ for sufficiently long times.

Models of anomalous transport

The Lorentz model. Anomalous transport emerges non-trivially in the Lorentz model.^{26–29} Here, a two-dimensional variant is used which consists of Brownian tracer particles exploring a disordered environment of randomly placed, overlapping circular obstacles of radius σ , which we choose as $\sigma = 3$ nm. The void space between the discs undergoes a continuum percolation transition at the critical obstacle density $n_c \sigma^2 \approx 0.35907$ (Ref. 30). The infinite cluster displays self-similar behaviour characterised by the fractal dimension $d_f = 91/48$, known from lattice percolation.²⁵ The tracer dynamics on this incipient infinite cluster is found to exhibit subdiffusion, $\delta r_\infty^2(t) \sim t^{2/d_w}$, with walk dimension $d_w \approx 2.878$ (Ref. 31), see inset of Fig. 1.

We have generated 1,600 trajectories of Brownian tracers with short-time diffusion coefficient $D_0 = 2.5 \mu\text{m}^2/\text{s}$, moving on the

infinite cluster at criticality. (In practice, we computed trajectories for particles on all clusters and evaluated the time-averaged mean-square displacement for each particle. Then, we selected those particles which did not show localisation based on a criterion for the local exponent of the mean-square displacement at very long times; only these particles contributed to the final average over independent trajectories.) Taking the divergent length scale into account, we have considered large systems of box length $L = 10^4 \sigma = 30 \mu\text{m}$ and have run the trajectories up to times of $t \approx 10^8 t_0$, where $t_0 = \sigma^2/D_0 = 3.6 \mu\text{s}$ is the natural time scale above which the diffusive motion is hindered by obstacles. The resulting correlation functions are invariant under time shift and do not display aging, in agreement with recent FCS experiments on crowded fluids.¹ For the *in-silico* experiment, we have evaluated the average in Eq. (6) for beam waists between 24 nm and 384 nm.

Fractional Brownian motion. Fractional Brownian motion (FBM) is a mathematical generalisation of the usual Brownian motion yielding a subdiffusive mean-square displacement, $\delta r^2(t) = 2dD_\alpha t^\alpha$, with the generalised diffusion constant D_α ; the distribution of the displacements $\Delta \mathbf{R}(t)$ remains Gaussian. The description of a microscopic process generating such a dynamics is challenging, one formulation involving fractional derivatives was given in terms of a generalised Langevin equation.³² Nevertheless, its “propagator” (van Hove function) can be calculated exactly to

$$P_{\text{FBM}}(r, t) = r^{-d} \widehat{P}_{\text{Gauss}}\left(r t^{-\alpha/2} / \sqrt{D_\alpha}\right) \quad (9)$$

where $\widehat{P}_{\text{Gauss}}(x) = (2\pi)^{-d/2} x^d \exp(-x^2/2)$ and d denotes the dimension of space. In particular, it satisfies the scaling form in Eq. (7) exactly. Brownian motion with normal diffusion is obtained in the limit $\alpha \rightarrow 1$, where D_α becomes the diffusion constant. The FCS function corresponding to FBM is given exactly by Eq. (5). For comparison with the Lorentz model, we have fixed α and D_α such that the mean-square displacements of both models coincide.

Results and Discussion

In the following, we will describe how FCS experiments with variable beam waist can provide insight into the microscopic dynamics and reveal spatially non-Gaussian, subdiffusive behaviour. We apply the generalised FCS theory from above to the exactly solvable FBM model and to the two-dimensional Lorentz model with Brownian tracers. We have generated FCS correlation functions as described in the previous section. The obtained curves are shown in Fig. 1 and exhibit a significantly stretched decay compared to normal diffusion. For the corresponding FBM model with identical mean-square displacement, the same trend, but a different shape of $G(t)$ is found. For both models, an increase of the beam waist w shifts the relaxation to later times, while the shape appears to be preserved.

Generalising the diffusion time in Eq. (1), we introduce the half-value time $\tau_{1/2}(w)$ as a function of the beam waist via the implicit definition $NG(\tau_{1/2}) = 1/2$. The FCS data suggest a phenomenological scaling property, $NG(t; w) = \widehat{G}(t/\tau_{1/2}(w))$, i.e., all curves can be collapsed by appropriate rescaling of time. In the following, we will rigorously derive the scaling form of the FCS function $G(t; w)$

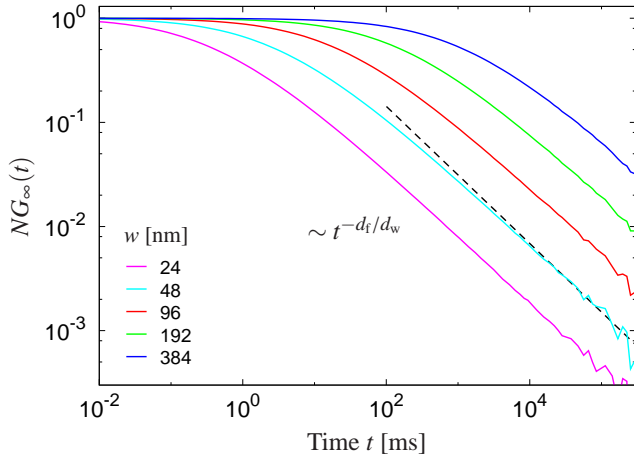


Fig. 2a: Simulated FCS data on double logarithmic scales; the data correspond to Fig. 1. The subdiffusive motion is mainly hidden in the tails of $G_\infty(t; w)$ at long times, $t/t_0 \gg (w/\sigma)^{d_w}$, which decay as a power law with exponent $\alpha = d_f/d_w$, indicated by the broken line.

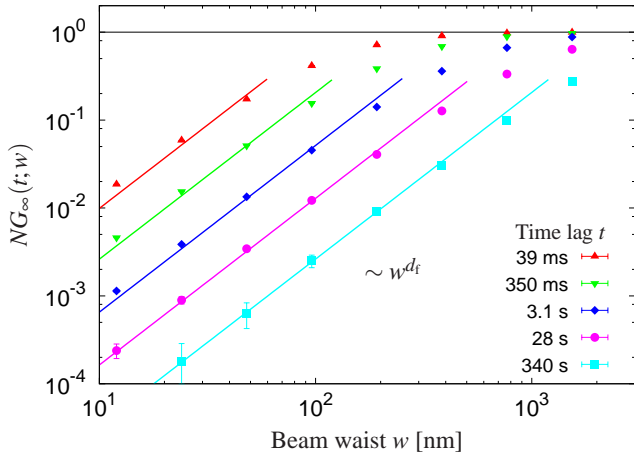


Fig. 2b: Simulated FCS data as a function of the beam waist w for different, but fixed time lags t ; the data correspond to Fig. 1. The regime $1 \ll w/\sigma \ll (t/t_0)^{1/d_w}$ is characterised by a power law increase with exponent d_f (solid lines), revealing the fractal spatial structure.

for the models under consideration. In particular, a thorough scaling analysis can discriminate whether or not a proposed theoretical model describes the spatio-temporal tracer dynamics contained in the FCS data.

Scaling of the FCS function.

The scaling properties of the FCS function are inherited from the van Hove function by means of the master formula, Eq. (6),

$$NG_\infty(t; w) = \int d^d r \exp(-r^2/w^2) P_\infty(r, t). \quad (10)$$

In case of the Lorentz model, one finds from Eq. (7) that

$$NG_\infty(t; w) = \widehat{G}_\infty(wt^{-1/d_w}) \quad (11)$$

for $w \gg \sigma$ and $t \gg t_0$, and similarly for the FBM model. For both models, these scaling forms imply a power-law divergence of the

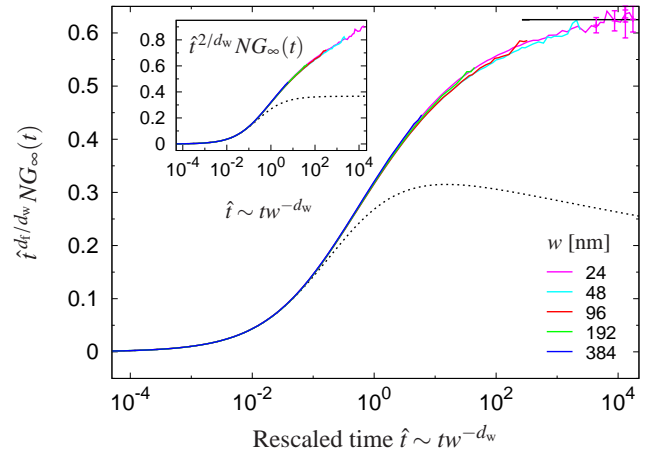


Fig. 3a: FCS functions $G_\infty(t)$ for various beam waists rescaled according to the scaling hypothesis, Eqs. (11) and (13). Solid lines correspond to the simulation data of Fig. 1, dotted lines to the solution for FBM. Inset: The assumption of Gaussian transport, Eq. (5), yields data collapse as well, but no saturation for large rescaled times.

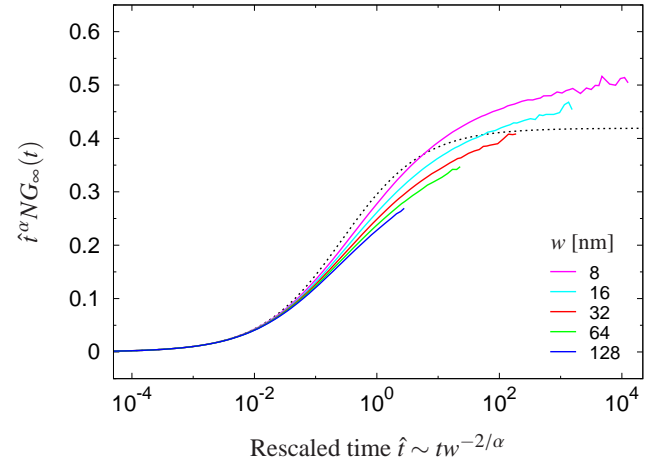


Fig. 3b: The assumption of spatially Gaussian transport, Eq. (5), does not lead to scaling of the FCS data for obstructed motion. The anomalous exponent $\alpha = 0.659$ is obtained from the long-time decay of $G_\infty(t)$ following Eq. (2). Dotted line: solution for the FBM model rescaled by the same procedure.

FCS half-value time in particular,

$$\tau_{1/2}(w) \sim w^{d_w} \quad \text{for } w \gg \sigma, \quad (12)$$

which is corroborated by the rescaling of $G(t; w)$ below. For *normal* diffusion on a mesh grid model, a corresponding relation has been derived.³³ In the regime $w \ll t^{1/d_w}$, the FCS experiment essentially probes the return probability $\Pi(t; w)$. Thus $\widehat{G}_\infty(x \ll 1) \sim x^{d_f}$, and a non-trivial power-law decay of the FCS function is predicted at long times,

$$G_\infty(t; w) \sim t^{-d_f/d_w}. \quad (13)$$

A double-logarithmic representation of our simulated FCS data indeed renders the final decay of $G_\infty(t; w)$ straight lines, see Fig. 2a. Different beam waists yield parallel lines, and the slopes are compatible with the expected value of $d_f/d_w = 0.66$.

The form of $\widehat{G}_\infty(\cdot)$ for small arguments further yields the fractal space dimension, $NG_\infty(t; w) \sim w^{d_f}$ for sufficiently large, fixed time

lag t . Thus, the structural properties can be obtained from the FCS data by fixation of the correlation time and sufficient variation of the beam waist. and the fractal dimension is directly accessible if the data are plotted on double-logarithmic scales, see Fig. 2b. The asymptotic regime is limited from below by the microscopic details of the system and from above by the crossover to the trivial behaviour, $NG_\infty(t; w \rightarrow \infty) = 1$. Within the remaining window, $1 \ll w/\sigma \ll (t/t_0)^{1/d_w}$, our FCS data reveal non-trivial power-law behaviour over 1.5 decades in space for the longest time lags, and the slope of the data corresponds to the fractal dimension $d_f = 1.9$ of the underlying space.

A simultaneous test of both the temporal decay of $G(t; w)$ and its dependence on the beam waist is provided by appropriate rescaling of the data. Figure 3a shows the FCS function divided by the predicted long-time decay as a function of the rescaled time $\hat{t} = (t/t_0)(w/\sigma)^{-d_w}$. The excellent data collapse strongly corroborates the scaling law of Eq. (11) and of the half-value time, Eq. (12). Simultaneously, the rectified data converge for $\hat{t} \rightarrow \infty$, validating the algebraic decay, Eq. (13).

This analysis is in stark contrast with the form of $G(t)$ obtained for subdiffusive motion and the assumption of spatially Gaussian transport, e.g., for the FBM model. It is instructive to discuss the implications for general dimension d . Then, Eq. (5) generalises to

$$NG_\infty^{\text{Gauss}}(t; w) = \left[1 + \delta r_\infty^2(t)/w^2\right]^{-d/2} \sim w^d t^{-d/d_w} \quad (14)$$

as $t \rightarrow \infty$, using $\delta r_\infty^2(t) \sim t^{2/d_w}$. The inset of Fig. 3a reveals that rectification with \hat{t}^{2/d_w} does not lead to saturation at long times, reflecting the fact that the decay of the FCS autocorrelation function for the obstructed motion decays with a different exponent than the inverse mean-square displacement. Nevertheless, the data still collapse on a single master curve, yet this shows merely that both the Gaussian ansatz and the critical scaling use the same reduced time \hat{t} . Conversely for the FBM result, Gaussian scaling yields convergence at long times, while the assumption of obstructed motion does not.

Let us perform the standard analysis for anomalous transport on our simulated FCS data, as suggested by Eq. (2). Fitting the long-time decay fixes the exponent to $\alpha = d_f/d_w$, which indeed yields a saturation in the rectification plot, see Fig. 3b. Interpreting this α as characteristic exponent of subdiffusion for the mean-square displacement, $\delta r_\infty^2(t) \sim t^\alpha$, and assuming Gaussian transport, Eq. (5), suggests the use of $\hat{t} \sim t w^{-2/\alpha}$ as scaling variable. However, then the data for our model system fan out for large times. Furthermore, it implies $\tau_{1/2}(w) \sim w^{2/\alpha} = w^{2d_w/d_f}$, contradicting Eq. (12). We conclude that the standard approach using only a single scaling exponent is not consistent for anomalous transport due to obstacles.

We close with the question when the widely used Eq. (2) is a valid description of the FCS correlation function. The equation is a specialisation of Eq. (5), which holds if and only if the distribution of displacements is Gaussian, i.e., solely determined by its second cumulant, $\delta r^2(t)$; this is a consequence of the master formula, Eq. (6). For spatially Gaussian transport, validity of Eq. (2) is then equivalent to a power-law increase of the mean-square displacement, $\delta r^2(t) \sim t^\alpha$. If the functional form of $\delta r^2(t)$ is different, e.g, if the dynamics exhibits a crossover from anomalous to normal diffusion at some crossover time scale t_x , Eq. (2) applies only

to shorter time lags, $t \ll t_x$. Since such a crossover is generically expected away from a critical point (see, e.g., the discussion in Ref. 18 and the simulation results in Refs. 26–29 and 31), the analysis of FCS data based on Eq. (5) appears more robust. Finally as a test of the Gaussian assumption, it would be essential to quantify the corrections to Eq. (5) by FCS experiments with variable beam waist.

Conclusions

We have shown that by systematic variation of the beam waist in FCS experiments, spatio-temporal information on the single-particle dynamics of complex systems can be collected. We have generalised the FCS theory beyond the assumption of spatially Gaussian transport and have derived a fundamental expression for the FCS correlation function, Eq. (6), which is a general starting point for the interpretation of experiments and which significantly facilitates theoretical and numerical work on FCS. In particular, it is straightforward to transfer our findings to the study of complex transport in other fields where FCS is widely employed, e.g., in physical chemistry and in polymer physics.

The obtained master formula for FCS reveals an analogy between FCS and time-resolved scattering techniques. It can be extended to the case where the concentration of the labeled particles is not dilute any more. Then a distinct part arises in addition to the self-part similar to the corresponding decomposition of the coherent intermediate scattering function. Likewise, one can easily account for the asphericity of the illuminated volume; yet this does not affect the scaling arguments presented in this work.

For subdiffusive motion due to obstacles, both the fractal nature of the underlying space and the anomalous transport can be revealed by FCS. We have developed a scaling theory for $G_\infty(t; w)$, which excellently describes our simulated data for the full range of investigated beam waists. These findings have been contrasted to fractional Brownian motion (FBM), an exactly solvable model for subdiffusion with different predictions for the scaling behaviour. The derived scaling properties should be experimentally accessible with modern nanoscopic optical methods.^{13,14} In particular, the spatial information provided by FCS can be used to experimentally distinguish different routes to anomalous transport.

We have demonstrated that a fit of the time-dependence of the FCS function for a single beam waist does not necessarily determine the walk dimension, which characterises the subdiffusive increase of the mean-square displacement, $\delta r^2(t) \sim t^{2/d_w}$. A more robust procedure would be based on measurements of the half-value time $\tau_{1/2}(w)$ of the normalised FCS correlations for a wide range of beam waists. Then, the exponent of subdiffusion may be obtained from the w -dependence $\tau_{1/2}(w) \sim w^{d_w}$, which is expected to hold for various models of anomalous transport, see Eq. (12). The knowledge of d_w would be the starting point for a scaling test of the full curves $G(t; w)$ similarly to Fig. 3a, which then would be completed by a characterisation of the decay at long times. The analysis by Wawrezynieck *et al.*¹⁰ is somewhat different from the one suggested here. Their ‘‘apparent diffusion time’’ τ_d^{app} corresponds to $\tau_{1/2}$ in our notation. Based on experimental data on the plasma membrane of COS-7 cells and on simulations, they find the phenomenological relation $\tau_{1/2} \sim w^2 + \text{const}$ and discuss im-

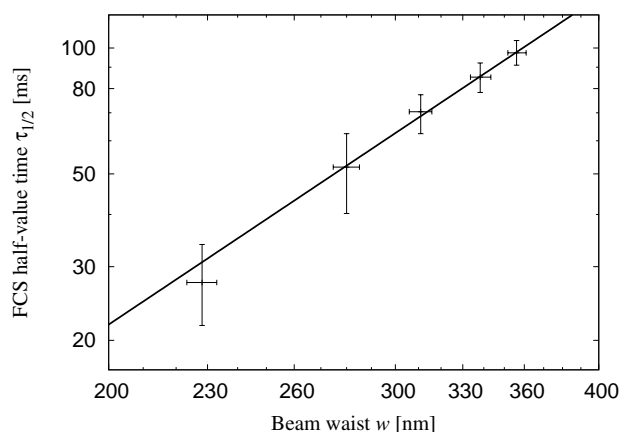


Fig. 4: Experimental FCS half-value times $\tau_{1/2}(w)$ from FCS measurements on the transmembrane protein GfR-GFP of COS-7 cells in a double-logarithmic representation; the data were taken from Fig. 4D of Ref. 10. The straight line indicates a power-law increase of the half-value times as function of beam waist, $\tau_{1/2} \sim w^{2.6}$.

plications of the offset as the data are extrapolated towards small beam waists, $w \rightarrow 0$. In Fig. 4, we have replotted their $\tau_{1/2}$ -data for the transmembrane protein GfR-GFP as function of the beam waist on double-logarithmic scales. The data points nicely follow a straight line in agreement with our power-law prediction, Eq. (12). Considering the error bars and the limited w -range, we obtain an estimate of the walk dimension d_w between 2.4 and 3.4; the most likely value is $d_w \approx 2.6$, implying an exponent of subdiffusion of $2/d_w \approx 0.77$. We find this observation rather encouraging with respect to the applicability of our approach and to the usefulness of FCS with variable beam waist for addressing the leading questions on anomalous transport.

Acknowledgment. We thank J. O. Rädler for insightful discussions on the experimental techniques. Financial support from the Deutsche Forschungsgemeinschaft via contract No. FR 850/6-1 and by the German Excellence Initiative via the program “Nanosystems Initiative Munich” (NIM) is gratefully acknowledged.

References

- 1 J. Szymanski and M. Weiss, *Phys. Rev. Lett.*, 2009, **103**, 038102.
- 2 M. Magdziarz, A. Weron, K. Burnecki and J. Klafter, *Phys. Rev. Lett.*, 2009, **103**, 180602.
- 3 Y. He, S. Burov, R. Metzler and E. Barkai, *Phys. Rev. Lett.*, 2008, **101**, 058101.
- 4 A. Lubelski, I. M. Sokolov and J. Klafter, *Phys. Rev. Lett.*, 2008, **100**, 250602.
- 5 M. J. Saxton, *Biophys. J.*, 2007, **92**, 1178–1191.
- 6 B. J. Sung and A. Yethiraj, *Phys. Rev. Lett.*, 2006, **96**, 228103.
- 7 S. T. Hess, S. Huang, A. A. Heikal and W. W. Webb, *Biochemistry*, 2002, **41**, 697–705.
- 8 P. Schwille, *Cell Biochemistry and Biophysics*, 2001, **34**, 383–408.
- 9 E. Gielen, M. van de Ven, A. Margineanu, P. Dedeker, M. V. der Auweraer, Y. Engelborghs, J. Hofkens and M. Ameloot, *Chem. Phys. Lett.*, 2009, **469**, 110–114.
- 10 L. Wawrezynieck, H. Rigneault, D. Marguet and P. F. Lenne, *Biophys. J.*, 2005, **89**, 4029–4042.

- 11 A. Masuda, K. Ushida and T. Okamoto, *Biophys. J.*, 2005, **88**, 3584–3591.
- 12 J. Wenger, F. Conchonaud, J. Dintinger, L. Wawrezynieck, T. W. Ebbesen, H. Rigneault, D. Marguet and P.-F. Lenne, *Biophys. J.*, 2007, **92**, 913–919.
- 13 S. W. Hell, *Science*, 2007, **316**, 1153–1158.
- 14 C. Eggeling, C. Ringemann, R. Medda, G. Schwarzmann, K. Sandhoff, S. Polyakova, V. N. Belov, B. Hein, C. von Middendorff, A. Schönle and S. W. Hell, *Nature*, 2009, **457**, 1159–1162.
- 15 G. Guigas, C. Kalla and M. Weiss, *FEBS Lett.*, 2007, **581**, 5094–5098.
- 16 D. S. Banks and C. Fradin, *Biophys. J.*, 2005, **89**, 2960–2971.
- 17 M. Weiss, H. Hashimoto and T. Nilsson, *Biophys. J.*, 2003, **84**, 4043–4052.
- 18 M. R. Horton, F. Höfling, J. O. Rädler and T. Franosch, *Soft Matter*, 2010, **6**, 2648–2656.
- 19 C. Selhuber-Unkel, P. Yde, K. Berg-Sorensen and L. B. Oddershede, *Phys. Biol.*, 2009, **6**, 025015.
- 20 I. Golding and E. C. Cox, *Phys. Rev. Lett.*, 2006, **96**, 098102.
- 21 A. Kusumi, C. Nakada, K. Ritchie, K. Murase, K. Suzuki, H. Murakoshi, R. S. Kasai, J. Kondo and T. Fujiwara, *Annu. Rev. Biophys. Biomol. Struct.*, 2005, **34**, 351–378.
- 22 I. M. Tolić-Nørrelykke, E.-L. Munteanu, G. Thon, L. Oddershede and K. Berg-Sørensen, *Phys. Rev. Lett.*, 2004, **93**, 078102.
- 23 B. J. Berne and R. Pecora, *Dynamic light scattering*, Wiley, New York, 1976.
- 24 J.-P. Hansen and I. McDonald, *Theory of Simple Liquids*, Academic Press, Amsterdam, 3rd edn., 2006.
- 25 D. ben Avraham and S. Havlin, *Diffusion and Reactions in Fractals and Disordered Systems*, Cambridge University Press, Cambridge, 2000.
- 26 F. Höfling, T. Franosch and E. Frey, *Phys. Rev. Lett.*, 2006, **96**, 165901.
- 27 F. Höfling and T. Franosch, *Phys. Rev. Lett.*, 2007, **98**, 140601.
- 28 F. Höfling, T. Munk, E. Frey and T. Franosch, *J. Chem. Phys.*, 2008, **128**, 164517.
- 29 T. Bauer, F. Höfling, T. Munk, E. Frey and T. Franosch, *Eur. Phys. J. Special Topics*, 2010, **189**, 103–118.
- 30 J. Quintanilla, S. Torquato and R. M. Ziff, *J. Phys. A*, 2000, **33**, L399–L407.
- 31 A. Kammerer, F. Höfling and T. Franosch, *Europhys. Lett.*, 2008, **84**, 66002.
- 32 K. L. Sebastian, *J. Phys. A*, 1995, **28**, 4305–4311.
- 33 N. Destainville, *Soft Matter*, 2008, **4**, 1288–1301.